This article has been accepted for publication in a future issue of this journal, but has not been fully edited. Content may change prior to final publication. Citation information: DOI 10.1109/MDAT.2020.2968286, IEEE Design and Test

Online Millimeter Wave Phased Array Calibration Based on Channel Estimation

Thomas Moon, Junfeng Gaun, Haitham Hassanieh
Electrical and Computer Engineering, University of Illinois at Urbana-Champaign, USA

***Abstract*—This article introduces a new over-the-air calibration method for millimeter wave phased arrays. Our method leverages the channel estimation process which is a fundamental part of any wireless communication system. By performing the channel estimation while changing the phase of an antenna element, the response of the element is obtained. Unlike prior work, our method includes all the system components and thus, spans the full chain. By overriding channel estimation, no additional circuits are required, and online calibration is possible without pausing the communication process. We tested our method on an eight-element-phased array at 24GHz which we designed and fabricated in PCB for verification.**

***Index Terms*—Phased Array, Millimeter Wave, Calibration, Beamforming, Over-the-air measurement**

I. Introduction

The surge of IoT and mobile devices has led to an explosive increase in demand for wireless bandwidth. This prompted the FCC to open multi-GHz of both license and unlicensed spectrum in the millimeter wave (mmWave) frequency bands above 24 GHz [1]. Millimeter wave is expected to deliver wireless link at fiber-like speeds of multi-Gbps and will play a central role in 5G cellular networks and future wireless LANs. However, mmWave signals attenuate quickly with distance. Hence, mmWave radios need to use directional antennas to focus the signal power and extend the range.

Phased arrays play a key role for directionality in mmWave. Substantial path loss at mmWave is compensated by the high directionality of phased arrays. Phased arrays allow us to electronically steer the direction of the beam in real-time in order to accommodate mobility and adapt to dynamic environments. A phased array works by changing the phase of the signal on each antenna element using a phase shifter. The phase shifter values are chosen in order to align the phase of the signals in a given direction θ to sum up constructively and beamform the signal towards θ.

However, mmWave phased arrays are extremely sensitive to small offsets due to the very small wavelength. Process variation and RMS phase error of the phase shifters can easily degrade the performance. Nanoscale CMOS transistors operating at mmWave frequency are more susceptible to long-term electrical-stress [2]. Temperature drifts also induce reliability degradations of the phase shifting [3]. The phased array without correcting these offsets and errors can beamform the signal in many directions. The poor beamforming limits the gain of the array and the performance of the mmWave system as well as interferes in other directions. Fig. 1 shows an example of the beam pattern of an 8 element phased array operating at 24 GHz before and after calibration. Without calibration, the beam is not directional. It has more than one main lobe and a significant number of sidelobes.

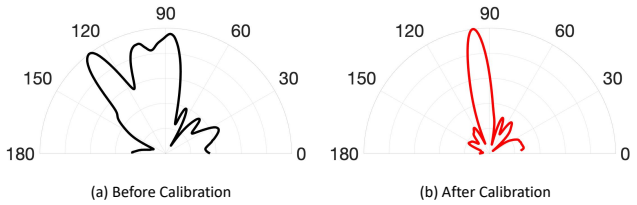

Fig. 1. Phased array beam pattern when directed towards 100° (a) before and (b) after calibration.

Unfortunately, calibrating the phased array requires expensive bench-equipment such as vector network analyzers (VNAs) which is not adequate for mass production. Such bench-equipment does not provide online calibration because recalibration is impossible after the array is used in the system. To reduce calibration cost and reliance on external test equipment, built-in self test (BIST) has been proposed as an alternative solution for phased array testing. In [4]–[6], on-chip BIST circuitry characterizes and calibrates the amplitude and phase of each channel of phased array. The approach in [7] applies code-modulation to each element in the array to allow parallel measurements using BIST architecture on the distribution network. Concurrent testing on all mixed/RF components in MIMO is demonstrated using multiple test tones generated by BIST circuit [8].

The BIST approach can generally achieve accurate measurements on the target system due to its proximity. However, it requires a special circuitry and its overhead becomes significant as the device size scales down at mmWave frequency. The BIST circuitry typically forms a wire connection to the components under test. Due to this limited access points, the mismatch or error beyond BIST coverage is not presented in the calibration process.The compatibility across different IC technology is another restriction to be considered in implementing BIST circuits. To address these issues, several methodology on over-the-air (OTA) calibration has been researched [9]–[11]. Some of them use amplitude-only measurement to estimate phase of each array element [10], while others use the mutual coupling of the array [9] or the scattering parameters of the probe antenna and the phased array to compute the excitations of the antenna elements [11]. Unfortunately, all these methods require a separate calibration process before the communication initiates and hence, cannot

This article has been accepted for publication in a future issue of this journal, but has not been fully edited. Content may change prior to final publication. Citation information: DOI 10.1109/MDAT.2020.2968286, IEEE Design and Test

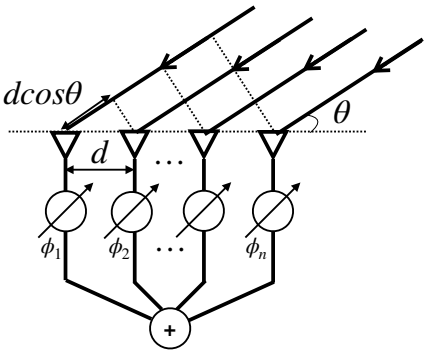

Fig. 2. **Phased Array System.** Phased array system can steer a beam at a direction θ by shifting the phase of signals.

correct the errors triggered by transistor aging, electrical stress or temperature changes.

This article introduces the online phased array calibration technique that enables calibrating the phased array during the communication process [12]. This allows us to continuously calibrate the phased array without the need for expensive equipment, specialized circuitry such as BIST or a separate calibration process that can only be done prior to using the phased array for communication. The key idea is to leverage the wireless *channel estimation protocol* that is an inherent part of any wireless communication system. By changing the phase shifter states and monitoring how the phase and magnitude of the wireless channel changes in response, we can calibrate the phased array to maximize the power at the desired direction and minimize the beam's sidelobes. Specifically, by performing the channel estimation while changing the phase of an antenna element, the phase response of the element can be estimated. The relative phase of the phased array can then be obtained by collecting all the estimated phase responses with a shared reference state which allows us to resolve the phase mismatches of the phased array. Our calibration method embraces all the array components such as power-divider, phase shifter, amplifier and antenna. Thus, the proposed method spans the full chain unlike prior work which is limited to a few selected components.

Since calibration takes place during the communication process, no additional measurements are required and in-field calibration is possible to adapt to system conditions such as temperature. We have implemented and tested our technique on a 24 GHz phased array with 8 antenna elements which we had designed and fabricated in PCB for verifications. Our results show that we can reduce the sidelobe leakage for the array by up to 7.3dB and our measured beam patterns prove the viability of our method.

II. Background

A. Phased Array

A phased array system is an array of antennas in which the relative phases of the signals can be controlled by the phase shifters as shown in Fig. 2. By changing the relative phases, the radiation pattern of the array is strengthened at a desired direction and suppressed at the rest. This allows the phased array system to electrically steer its radiation pattern without mechanically moving the antennas.

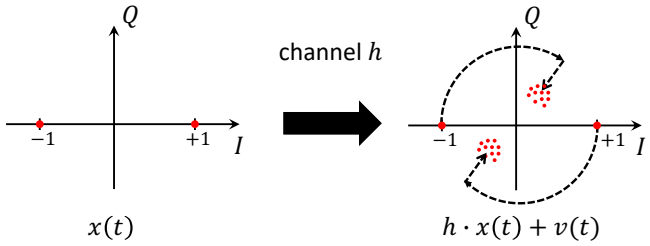

Fig. 3. **Channel Distortion.** The channel attenuates, phase-rotates, and adds the AWGN noise on the signal. To correctly demodulate the original symbols, the channel distortion should be corrected beforehand.

If a signal is arrived at a certain angle, θ, the distance traveled by the signal at the antenna element will be differed by $d\cos\theta$ with its neighbor element where d is the displacement of the antenna elements. Mathematically, the power P of signals arriving along the direction θ can be written as:

$$P(\theta) = \sum_{n=1}^{N_p} e^{j2\pi \frac{nd\cos\theta + \phi_n}{\lambda}} \tag{1}$$

where ϕ_n is the phase change by the n-th phase shifter, N_p is the total number of the antenna elements, and λ is the wavelength of the signal. By setting the phase shift ϕ_n equal to $-nd\cos\theta$, the power is maximized at the direction θ, and thereby the beam pattern is steered to the desired direction.

Note that a small phase error in ϕ_n can be amplified when the signal wavelength (λ) is a small value. In mmWave signal, the wavelength is 5-10 times shorter (0.5-1cm) than WiFi or LTE signal (5-10cm). Hence, the phased array system for mmWave is more sensitive in phase error than the sub-6GHz system.

B. Channel Estimation & Correction

In wireless communication, the received signal is corrupted by the channel response such as attenuation, phase shift, and noise. The channel impulse response (CIR), h, can be expressed as:

$$h = \alpha e^{-j2\pi f\tau} \tag{2}$$

where α is the magnitude response, f is the frequency, and τ is the time-of-flight between the transmitter and the receiver. The signal at the receiver, $y(t)$, through the channel h is

$$y(t) = h \cdot x(t-\tau) + v(t) \tag{3}$$

$$= \alpha e^{-j2\pi f\tau} x(t-\tau) + v(t) \tag{4}$$

where $x(t)$ is the transmitted signal and $v(t)$ is the additive Gaussian white noise (AWGN). The channel not only attenuates the signal, but rotates the phase by $2\pi f\tau$. Fig. 3 shows an example how the channel distorts the transmitted signal. In the example, the symbols are modulated by binary phase shift keying (BPSK) which encodes bit 1 as +1 and bit 0 as -1 in the IQ constellation. After the symbols pass through

the channel h, the received symbols are attenuated and phase-rotated and added by the noise. Notice that the receiver can fail decoding the correct bits due to the phase rotation even with high signal-to-noise ratio (SNR).

To correct the distortion from the channel, the receiver needs to estimate the channel h first. To do this, the transmitter sends a *training sequence* which is also known in priori by the receiver. The channel h can be estimated as:

$$\hat{h} = \frac{1}{N}\sum_{k=1}^{N}\frac{y[k]}{x[k]} \tag{5}$$

where N is the total number of the training sequence, and $y[k]$ and $x[k]$ are the k-th symbol of the transmitter and the receiver, respectively.

C. Channel Estimation in OFDM

The transmitted signal over the wireless channel suffers inter-symbol interference (ISI) due to multipath channel effect and frequency-selective fading. Equation 4 assumes a single path between the transmitter and receiver. In the presence of multipath, Equation 4 is extended by

$$y(t) = h(t) * x(t) + v(t) \tag{6}$$

$$= \sum_{k} h(\tau_k)x(t-\tau_k) + v(t) \tag{7}$$

The channel h is not a single number anymore. Since h is convolved with the input signal x, it is not possible to be estimated by Equation 5. In conventional single-carrier system, complex time-domain equalization techniques is required to deconvolve the channel h from the received training sequence. The main advantage of OFDM over single-carrier system is that it can deal with the multipath channel without the complex equalizations.

OFDM divides a spectrum band into many small and partially overlapping subcarriers, and modulates the symbols on the subcarriers. The subcarriers are chosen to be orthogonal so that the inter-carrier interference sums up zero. The OFDM output signal at the transmitter is given by

$$x(t) = \sum_{k=0}^{N-1} X(f_k)e^{j\frac{2\pi f_k t}{N}} \tag{8}$$

where f_k is the k-th subcarrier frequency. The above equation is an N-point inverse discrete Fourier transform (IDFT), which can be implemented in Fast Fourier transform requiring only $O(N\log N)$ computation. Once the transmitter performs the IFFT to convert the symbols in the frequency domain to N time domain samples, the receiver converts the signal back to the frequency domain using the FFT, where each subcarrier is demodulated independently.

Let $X_{i,k}$ is the transmitted OFDM symbol at the time index i and the frequency index k. The received OFDM symbol $Y_{i,k}$ can be written as

$$Y_{i,k} = H_k X_{i,k} + w \tag{9}$$

where H_k is the frequency response of the channel at k-th frequency index and w is the frequency-domain AWGN. If a training OFDM symbol at $i = -1$ (also called a *preamble*) is sent before the data OFDM symbols ($i = 0, 1, 2, ...$), H_k can be estimated by the Least Squares (LS) method as:

$$\hat{H_k} = \frac{Y_{-1,k}}{X_{-1,k}} \tag{10}$$

Notice that H is obtained through dividing the received symbols (Y) by the transmitted symbols (X) without a complicated deconvolution process. This is possible because the symbol is sent in the frequency-domain and the channel H is *multiplied* with the transmitted symbols. Therefore, the channel estimation in OFDM can be performed in much simpler way than the conventional single-carrier system. This is the reason we choose OFDM for our communication scheme in the proposed method.

III. Proposed Method

A. Channel including Phased Array

Consider the phased array system of N_p number of antenna elements transmitting OFDM symbols. We can write the received OFDM symbols as:

$$Y = HX \tag{11}$$

$$= \left(a_0 e^{j\phi_0} + \sum_{n=1}^{N_p} a_n e^{j\phi_n}\right)X \tag{12}$$

where a_n and ϕ_n are the magnitude and phase response of n-th antenna element, respectively. For the sake of simplicity, the time and frequency index (i and k) are omitted. $a_0 e^{j\phi_0}$ represents the leakage signal that is emitted by power divider/combiner or the RF devices, not by the antenna elements. The leakage signal is undesirable but difficult to be completely removed.

Fig. 4 (a) demonstrates how the phased array contributes to the channel. As described in Equation 12, the total channel H is the summation of the response of the phase shifters and the leakage signal. If one element changes its phase from 0 to 2π, the total channel response will make a full rotation (the red circle in Fig. 4 (a)). In other words, the response of the phase shifter can be analyzed by the trajectory of the total channel response.

Note that Equation 12 omits the frequency index k. The channel H is estimated at every subcarrier frequency as described in the background section. During the channel estimation, the channel from H_0 to H_{N-1} is obtained simultaneously. Therefore, the channel response over the bandwidth is measured at once. This potentially means that wideband calibration is possible as long as the OFDM bandwidth supports.

B. Challenges

In practice, the magnitude and phase response of antenna element has a more complicated form than described in Equation 12. If we look closely into one element, the response of one element can be written as a function of the control state, s:

$$f_n(s) = a_n(s)e^{j\phi_n(s)+\varphi_n} \tag{13}$$

This article has been accepted for publication in a future issue of this journal, but has not been fully edited. Content may change prior to final publication. Citation information: DOI 10.1109/MDAT.2020.2968286, IEEE Design and Test

where φ_n represents the phase mismatch with the reference phase shifter (here we set the first phase shifter as the reference). The control state s is an input for the phase shifter that changes the output phase. The state can be either continuous (e.g. voltage) or discrete (e.g. digital bus) depending on the architecture of the phase shifter.

There are two challenges: First, the function $a_n(s)$ and $\phi_n(s)$ representing the unique characteristic of each phase shifter are not identical over the other elements. In other words, the magnitude and phase are unknown at a given state. Second, even all the phase shifters are assumed to be identical, the phase mismatch term, φ_n, is unknown in general. The phase mismatch comes from the variation of other RF components such as power divider/combiner or antenna patches. They are usually independent with the phase shifters, and thus independent with the state s.

In this paper, we assume the response of the phase shifters are not randomly different but share a similar characteristic. In section III-C, the shared model will assist to enhance the estimation. Consequently, the phase mismatch can be resolved in section III-D.

C. Model-assisted Phase Estimation

We assume the phase shifters shares a common magnitude and phase response that is known in priori. However, due to manufacturing variation and mismatch, their output measurements are not identical. For example, two phase shifters can share a common response but can create two different channel constellations. The actual constellation of the phase shifters can be different due to 1) different magnitude and phase response to control state, 2) relative phase offset, and 3) noise. In practice, the magnitude response is not flat over the phase shifts. Thus, the constellation does not necessarily form a circle while the phase is shifting from 0 to 2π, which makes the estimation difficult.

Suppose (c^i, c^q) is the unknown center of the trajectory on the constellation and $(i(1), q(1)), (i(2), q(2)), ..., (i(N_s), q(N_s))$ are the measurements at N_s discrete phase states. The goal is to find the best estimate of the center given the measurements and the model response. Consider the vectors $\vec{\mathbf{v}}(1) = [i(1), q(1)]^T - [c^i, c^q]^T$ and $\vec{\mathbf{v}}(2) = [i(2), q(2)]^T - [c^i, c^q]^T$ as shown in Fig. 4 (b). $\vec{\mathbf{v}}(2)$ can be obtained by rotating θ_2 and scaling c_2 on $\vec{\mathbf{v}}(1)$. It can be described as

$$\mathbf{S}(c_2)\mathbf{R}(\theta_2)\vec{\mathbf{v}}(1) = \vec{\mathbf{v}}(2) \tag{14}$$

$$\mathbf{S}(c_2)\mathbf{R}(\theta_2)\begin{bmatrix} i(1)-c^i \\ q(1)-c^q \end{bmatrix} = \begin{bmatrix} i(2)-c^i \\ q(2)-c^q \end{bmatrix} \tag{15}$$

$$\begin{bmatrix} i(2) \\ q(2) \end{bmatrix} - \mathbf{S}(c_2)\mathbf{R}(\theta_2)\begin{bmatrix} i(1) \\ q(1) \end{bmatrix} = \Big(\mathbf{I} - \mathbf{S}(c_2)\mathbf{R}(\theta_2)\Big)\begin{bmatrix} c^i \\ c^q \end{bmatrix} \tag{16}$$

where $\mathbf{S}(c)$ is the scaling matrix $\begin{bmatrix} c & 0 \\ 0 & c \end{bmatrix}$ and $\mathbf{R}(\theta)$ is the rotation matrix $\begin{bmatrix} \cos\theta & -\sin\theta \\ \sin\theta & \cos\theta \end{bmatrix}$. Note that matrix S and R are determined by the model, and thus they are given in priori.

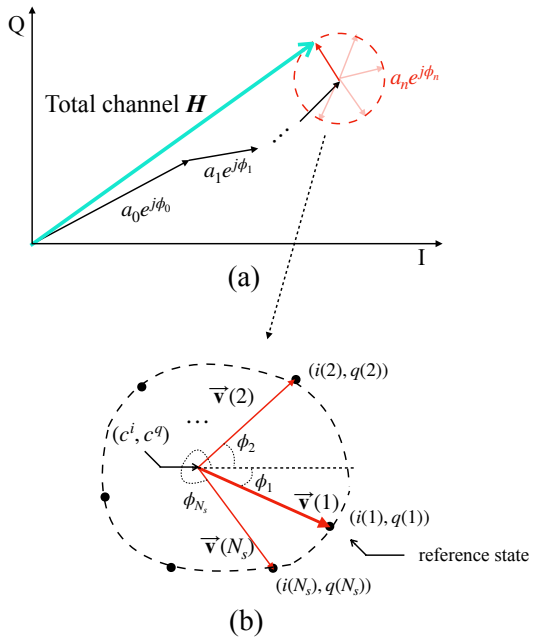

Fig. 4. **Channel Estimation Constellation.** (a) The overall channel response is a linear combination of the antenna elements. (b) The response of phase shifter is determined by a given model. Changing the control state of the phase shifter will move the channel response.

By defining

$$\mathbf{y_m} = \begin{bmatrix} i(m) \\ q(m) \end{bmatrix} - \mathbf{S}(c_m)\mathbf{R}(\theta_m)\begin{bmatrix} i(1) \\ q(1) \end{bmatrix} \tag{17}$$

$$\mathbf{a_m} = \mathbf{I} - \mathbf{S}(c_m)\mathbf{R}(\theta_m) \tag{18}$$

, Equation 16 can be written as:

$$\mathbf{y_2} = \mathbf{a_2}\mathbf{x} \tag{19}$$

where $\mathbf{x}$ is the unknown center $\begin{bmatrix} c^i \\ c^q \end{bmatrix}$.

The 2-by-2 system in Equation 19 can be expanded to $2(N_s-1)$-by-2 system by observing all N_s constellation points as follows:

$$\begin{bmatrix} \mathbf{y_2} \\ \mathbf{y_3} \\ \vdots \\ \mathbf{y_{N_s}} \end{bmatrix} = \begin{bmatrix} \mathbf{a_2} \\ \mathbf{a_3} \\ \vdots \\ \mathbf{a_{N_s}} \end{bmatrix}\mathbf{x} \tag{20}$$

$$\mathbf{Y} = \mathbf{A}\mathbf{x} \tag{21}$$

The above system is linearly over-determined, $2(N_s-1)$ observations for two unknowns. It is a linear regression problem that estimates the unknown model parameter, $\mathbf{x}$, from the data. Linear least square estimation minimized the sum of squared residuals:

$$\hat{\mathbf{x}} = (\mathbf{A^T}\mathbf{A})^{-1}\mathbf{A^T}\mathbf{Y} \tag{22}$$

where $\hat{\mathbf{x}} = \begin{bmatrix} \hat{c^i} \\ \hat{c^q} \end{bmatrix}$ is the least squared estimation for the unknown center. This process is repeated for all N_s number of phase shifters.

This article has been accepted for publication in a future issue of this journal, but has not been fully edited. Content may change prior to final publication. Citation information: DOI 10.1109/MDAT.2020.2968286, IEEE Design and Test

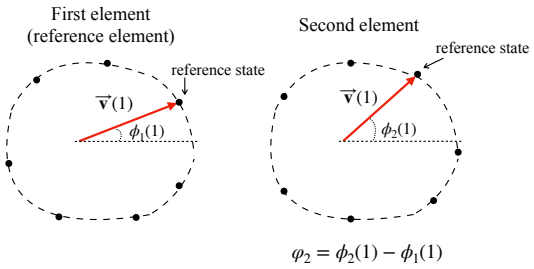

Fig. 5. **Phase Mismatch.** The phase mismatch is obtained by comparing the phases at the reference state.

D. Phase Mismatch Calibration

Once we found the center of the n-th element, the magnitude and phase of state m can be calculated as:

$$a_n(m) = |\vec{\mathbf{v}}_n(m)| \tag{23}$$

$$\phi_n(m) = \angle\vec{\mathbf{v}}_n(m) \tag{24}$$

where $\vec{\mathbf{v}}_n(m)$ is the vector measured by the *n*-th phase shifter at the state *m*.

The relative phase mismatch across the antenna elements is calculated by comparing the phase with the reference element. For example, we set the first element as the reference element and the first state as the reference state. The relative phase between the reference element and the n-th element is equal to the phase difference at the reference state as:

$$\varphi_n = \phi_n(1) - \phi_1(1) \tag{25}$$

Fig. 5 shows an example of phase mismatch between two elements. It is a reasonable assumption that the phase mismatch is independent with the control state and has a fixed constant offset because the source of the mismatch comes from the passive components such as power divider and patch antenna.

E. Handling Synchronization Offsets

When the transmitter and the receiver encounter a significant carrier frequency offset (CFO) or sampling frequency offset (SFO), they should be corrected as well in order to achieve a correct channel estimation. The estimation of the CFO/SFO will be affected while the phase shifters change their phase. This issue can be resolved by adding a single static antenna on each Tx and Rx to form a static channel (or if they are MIMO system, one of channel can be reserved for the static channel). The CFO/SFO estimation on the static channel can be used to cancel the frequency offset between Tx/Rx, and thus the synchronization can be achieved during the phase changes.

IV. Hardware Implementation

To evaluate the proposed method, a mmWave phased array system is designed and built. The hardware block diagram is shown in Fig. 6. The hardware system is implemented by the commercial off-the-shelf components. NI USRP-2920 transmits/receives OFDM baseband signals and processes baseband signal. We use HMC815 and HMC977 evaluation board for 24GHz I/Q up-converter and down-converter, respectively. The up/down-converters include an internal power amplifier/LNA, an IQ mixer, and a frequency doubler. LMX2594 PLL evaluation board generates the LO signal at 11GHz for the IQ up/down-converters. A prototype phased array test board is fabricated on printed circuit board (PCB) on Rodgers substrate as shown in Fig. 7 (b). The power divider and the patch antennas were simulated and designed by Advanced Design System. The phased array board includes 8 antenna elements spaced by $\lambda/2$. The RF input signal is splitted by the power divier and fed into 24GHz analog phase shifters (HMC-933). The control voltage for the phased shifter is generated by a 8-bit DAC (AD7228A). The DAC is controlled by Arduino Duo micro-controller which is synchronized with USRP through the PC. The phased array is used for the transmitter antenna in this work, but there is no restriction that the array is used in the receiver side. We use a K-band horn antenna from SAGE for the receiver antenna. The horn antenna has 22dBi gain and 12 degree 3dB beamwidth. Theoretically, it is possible that both transmitter and receiver use the phased array and calibrate them one-by-another. However, we use a horn antenna to simplify the experiment setup.

V. Experimental Results

The proposed calibration method is evaluated on 8-element 24GHz phased array. To calibrate the phased array on the transmitter, we use the horn antenna at the receiver side facing toward transmitter. The control voltage is swept from 0V to 10V while the transmitter and the receiver are communicating OFDM packets. Fig. 8 shows the measured channel constellation at two different elements. We import the magnitude and phase specification of the phase shifters (HMC-933) and estimate the center for the trajectory. We run the calibration 10 times for each 8 element. The gain and phase estimated for the 8 elements by the channel estimation is plotted in Fig. 9. The red circles represents the specification of the phase shifter. The figure shows that a few phase shifters have a huge phase offset more than 100 degree. This phase mismatch will degrade the beam pattern without a proper calibration. In Fig. 10, the standard deviation of the gain and phase calibration result is shown. The result shows the calibration is stable enough that the standard deviation of the gain and phase are less than 1dB and 5 degree, respectively.

To evaluate the beam pattern with calibration, the phased array is mounted on a pole equipped with a precise step motor. We setup the phase shifters of the array to steer at a specific angle, then we rotate the phased array antenna from 0-180 degrees while the horn antenna is receiving the transmitted signal. We measure the received power at each angle which gives us the radiation pattern. In Fig. 12, we set the phased array to steer the beam at 9 different angles (50-130 degree, 10 degree step) and compare the beam patterns with and without calibration. For the sake of clarification, the peak magnitude is normalized in both cases. In general, the peak power without the calibration is smaller than with the calibration because the signal power is not focused at one direction. The beam pattern with calibration shows that the main lobe is narrower and the side lobe levels are lower than without calibration. For each measured beam pattern, we calculate the side lobe

This article has been accepted for publication in a future issue of this journal, but has not been fully edited. Content may change prior to final publication. Citation information: DOI 10.1109/MDAT.2020.2968286, IEEE Design and Test

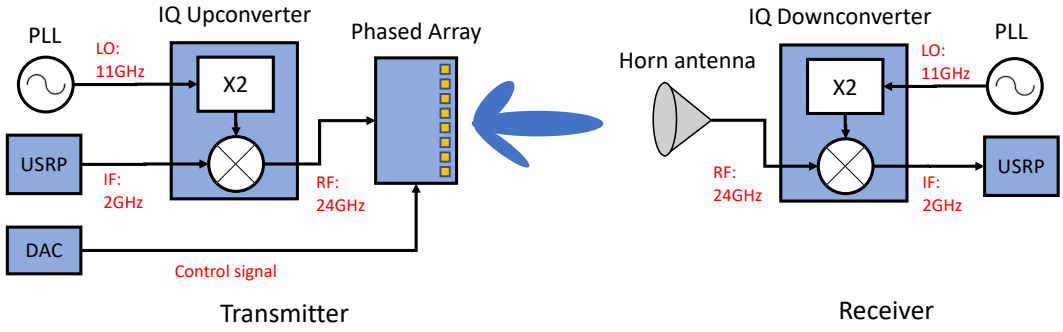

Fig. 6. **Hardware Block Diagram.** Block diagram of the mmWave transmitter and receiver.

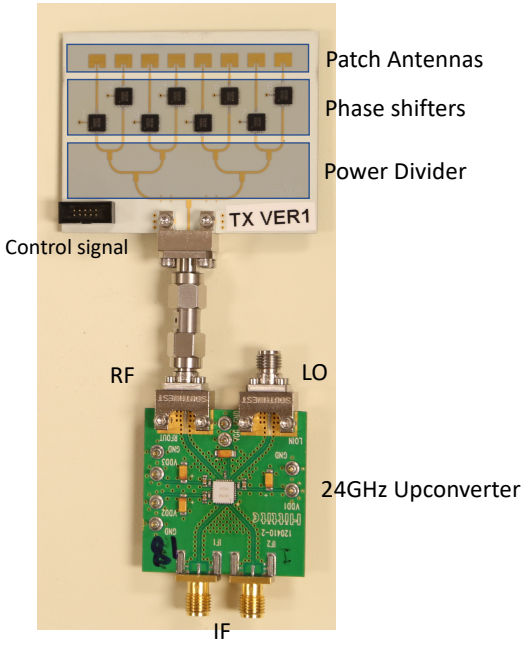

Fig. 7. **Phased Array and Up-converter Hardware.** Each 24GHz phase shifter is connected to a patch antenna. The control voltage is provided by an external DAC through the connector.

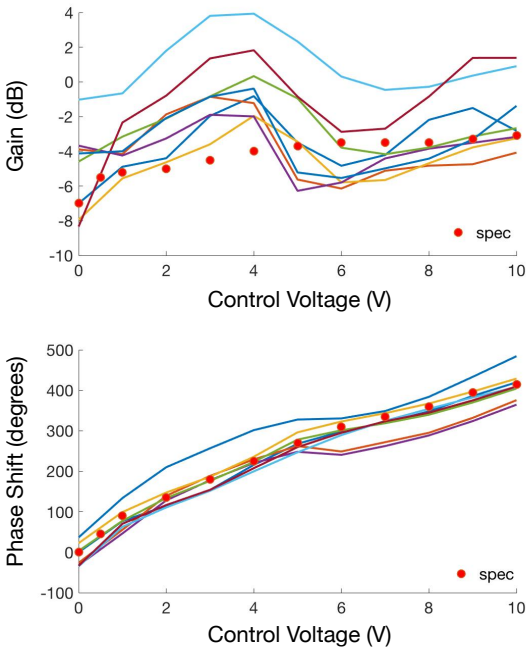

Fig. 9. **Estimated Gain and Phase.** The figure shows the estimated gain and phase of the 8 phase shifters over the control voltage. The red dots shows the specification of the phase shifter.

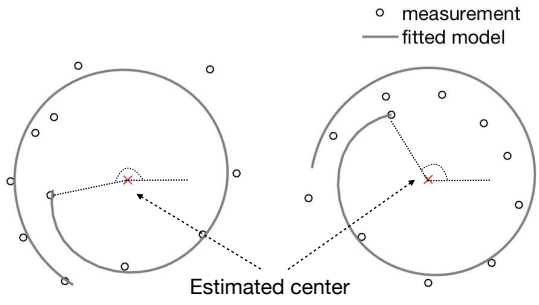

Fig. 8. **Measured Channel Estimation and Model.** The figure shows the channel estimation from two phase shifters with the fitted model. The relative phase can be evaluated by comparing the reference state.

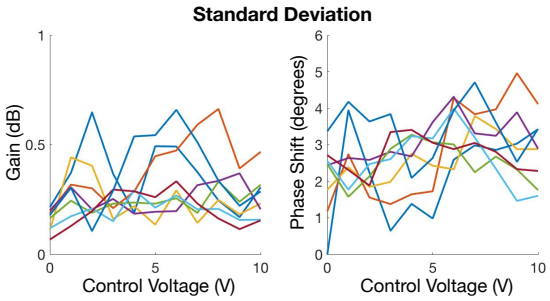

Fig. 10. **Stability of Calibration.** Standard deviation of calibration result. The figure shows that the calibration is stable within 1dB gain deviation and 5 degree phase deviation.

level (SLL) which is the side lobe power relative the main lobe. Higher SLL means that the antenna leaks more power outside the main lobe. Fig. 11 compares the CDF of SLL with and without calibration. The 90th percentile of SLL is -1.3dB without calibration, while it reduces to -8.6dB with calibration. The result implies that calibration reduces side lobe power and improves the directionality of the phased array.

We observed that the beam patterns with calibration still have higher side lobes than the theoretical value. The main reason for this is because of the magnitude mismatch between

This article has been accepted for publication in a future issue of this journal, but has not been fully edited. Content may change prior to final publication. Citation information: DOI 10.1109/MDAT.2020.2968286, IEEE Design and Test

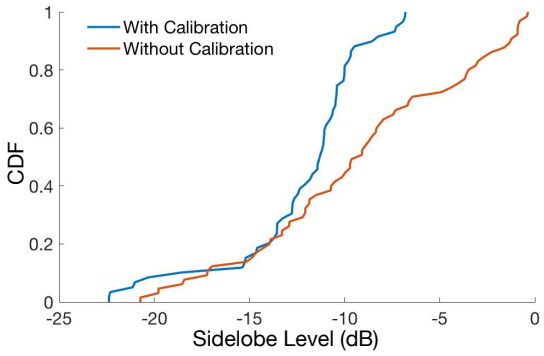

Fig. 11. **Performance of Calibration.** CDF of sidelobe level relative to the main beam with and without calibration. The figure shows that calibration significantly reduces the radiation outside of the main beam.

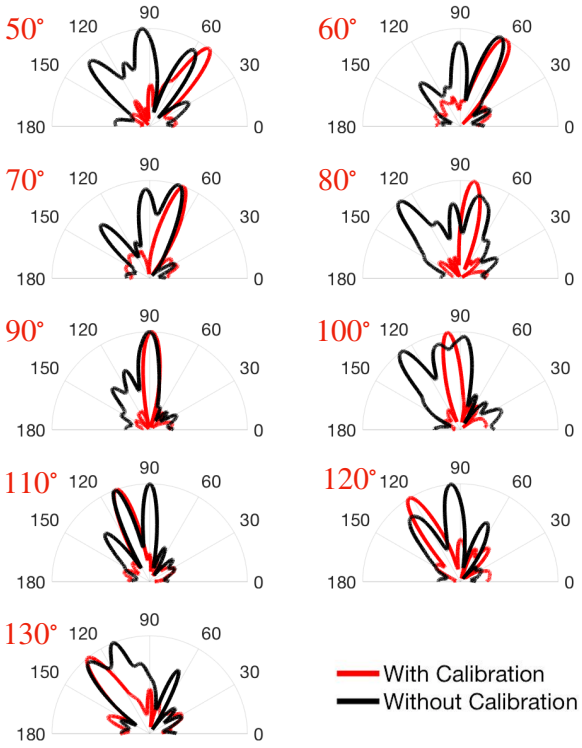

Fig. 12. **Beam Patterns.** The measured beam patterns steered at 9 different angles are shown. The beam patterns before (black) and after (red) calibration are compared. The peak magnitude is normalized for better visualization.

the elements. We do not calibrate the magnitude mismatch in this work because our hardware does not support the control over the magnitude for each element. This problem will be further studied in the future work.

VI. Conclusion

In this article, we introduce a new online OTA calibration method for mmWave phased array. Phase calibration is extremely difficult in mmWave system due to its very small wavelength. Our method leverages the channel estimation protocol which is an essential part of any wireless communication. By measuring the phase response of the array while changing the phase shifter states, we can estimate the phase mismatches and calibrate the phased array. This allow us continuous calibration not necessarily to interrupt the communication without extra circuits. We implemented an 8-element 24GHz phased array system to evaluate our calibration. The hardware measurement results prove that our calibration is capable of compensating the phase mismatches and improves the beam pattern by reducing SLL.

References

[1] A. Pai, "Keeping up a fast pace on spectrum," https://www.fcc.gov/news-events/blog/2018/10/01/keeping-fast-pace-spectrum, FCC, 2018.

[2] J. Yuan, Y. Xu, S. Yen, Y. Bi, and G. Hwang, "Hot carrier injection stress effect on a 65 nm lna at 70 ghz," *IEEE Transactions on Device and Materials Reliability*, vol. 14, no. 3, pp. 931–934, 2014.

[3] C.-Y. Kim, D.-W. Kang, and G. M. Rebeiz, "A 44–46-ghz 16-element sige bicmos high-linearity transmit/receive phased array," *IEEE Transactions on Microwave Theory and Techniques*, vol. 60, no. 3, pp. 730–742, 2012.

[4] S. Y. Kim, O. Inac, C.-Y. Kim, and G. M. Rebeiz, "A 76–84 ghz 16-element phased array receiver with a chip-level built-in-self-test system," in *Radio Frequency Integrated Circuits Symposium (RFIC), 2012 IEEE*. IEEE, 2012, pp. 127–130.

[5] O. Inac, F. Golcuk, T. Kanar, and G. M. Rebeiz, "A 90–100-ghz phased-array transmit/receive silicon rfic module with built-in self-test," *IEEE Transactions on Microwave Theory and Techniques*, vol. 61, no. 10, pp. 3774–3782, 2013.

[6] J. W. Jeong, J. Kitchen, and S. Ozev, "A self-compensating built-in self-test solution for rf phased array mismatch," in *Test Conference (ITC), 2015 IEEE International*. IEEE, 2015, pp. 1–9.

[7] K. Greene, V. Chauhan, and B. Floyd, "Built-in test of phased arrays using code-modulated interferometry," *IEEE Transactions on Microwave Theory and Techniques*, vol. 66, no. 5, pp. 2463–2479, 2018.

[8] S. Deyati, B. J. Muldrey, B. Jung, and A. Chatterjee, "Concurrent built in test and tuning of beamforming mimo systems using learning assisted performance optimization," in *Test Conference (ITC), 2017 IEEE International*. IEEE, 2017, pp. 1–10.

[9] H. M. Aumann, A. J. Fenn, and F. G. Willwerth, "Phased array antenna calibration and pattern prediction using mutual coupling measurements," *IEEE Transactions on Antennas and Propagation*, vol. 37, no. 7, pp. 844–850, 1989.

[10] R. Long, J. Ouyang, F. Yang, W. Han, and L. Zhou, "Fast amplitude-only measurement method for phased array calibration," *IEEE Transactions on Antennas and Propagation*, vol. 65, no. 4, pp. 1815–1822, 2017.

[11] ——, "Multi-element phased array calibration method by solving linear equations," *IEEE Transactions on Antennas and Propagation*, vol. 65, no. 6, pp. 2931–2939, 2017.

[12] T. Moon, J. Gaun, and H. Hassanieh, "Online millimeter wave phased array calibration based on channel estimation," in *2019 IEEE 37th VLSI Test Symposium (VTS)*. IEEE, 2019, pp. 1–6.